Simultaneous thermographic and optical recording media examination of the first oxide spallation event from the surface of an austenitic stainless steel

Mobbs, Rebecca-Louise; Ramsay, Joshua; Reynolds, Tom; Gray, Simon ; Osgerby, Steven; Taylor, Mary

DOI:
10.1016/j.corsci.2020.109103

Document Version
Peer reviewed version

Citation for published version (Harvard):
Mobbs, R-L, Ramsay, J, Reynolds, T, Gray, S, Osgerby, S & Taylor, M 2021, 'Simultaneous thermographic and optical recording media examination of the first oxide spallation event from the surface of an austenitic stainless steel', *Corrosion Science*, vol. 179, 109103, pp. 1-13. https://doi.org/10.1016/j.corsci.2020.109103

Corrosion Science

Simultaneous Thermographic and Optical Recording Media Examination of the First Oxide Spallation Event from the Surface of an Austenitic Stainless Steel

--Manuscript Draft--

Manuscript Number:	CORSCI_2020_1757R1
Article Type:	Full Length Article
Keywords:	Spallation; steam oxidation; Delamination; strain energies
Corresponding Author:	Mary Taylor University of Birmingham Birmingham, United Kingdom
First Author:	Rebecca-Louise Mobbs
Order of Authors:	Rebecca-Louise Mobbs
	Joshua Ramsay
	Thomas Reynolds
	Simon Gray
	Steven Osgerby
	Mary Taylor
Abstract:	Spallation of oxides grown on TP347H FG in air-saturated steam at 923 K for 50 – 1000 hours was investigated using a newly developed technique termed: Simultaneous Thermographic and Optical Recording Media Examination (STORME), recording the temperature disturbance resulting from delamination and spallation, during cooling, using Infra Red and video cameras. For the first time, the radius of the delamination site was measured experimentally at the point of buckle formation and followed during growth to the point of spallation. Collection of the exact spalled fragment was possible. The strain energies at each stage were calculated and a Spallation Map constructed.
Response to Reviewers:	Comments from the editors and reviewers: -Reviewer 1 - This is a very carefully prepared paper that addresses the issue of buckling and spalling of oxide scales in a very detailed and competent manner. The new technique described has an intriguing potential to monitor the progress of scale damge during cooling and complements nicely with other techniques that characterize the mechanical limits of oxide scales. It is recommended that the paper be published in its present form. It is, however, recommended that fig. 11 is described in some more detail as it does not seem to be perfectly clear what the different lines and symbols mean in this figure. The authors thank the reviewer for these kind words. We also thank the reviewer for the opportunity to improve on Figure 11, the Spallation Map. This has now been completed with improvements, with an improved description within the text, all changes have been highlighted in red in the revised manuscript and the caption for Figure 11. In addition, the acknowledgement has been extended to include the work performed at the NPL where the idea of using IR cameras to detect heat flow from surfaces came from. That would was on thermal barrier coating at room temperature using low temperatures. We were very pleased to find the technique worked for us during cooling.

Metallurgy and Materials
The University of Birmingham
Birmingham B15 2TT

Dear Editor,

Please accept this manuscript for consideration for publication in Corrosion Science. It includes a new technique devised to detect and measure delaminated areas within thermally grown oxides formed under steam conditions on an austenitic steel. The parameters collected during the cooling stage, of temperature and diameter, have been input into equations described by Prof Hugh Evans, and a spallation map plotted. Hugh was the primary supervisor on this project but, unfortunately, was unable to see the paper through to completion. We, the authors, have taken it upon ourselves to perform this task and present this as a tribute to Hugh.

We believe that the content of this paper is appropriate for your journal and hope that you will give it due consideration.

Yours faithfully

Dr Mary Taylor

Response to reviewer's comments

Comments from the editors and reviewers:
-Reviewer 1

- This is a very carefully prepared paper that addresses the issue of buckling and spalling of oxide scales in a very detailed and competent manner. The new technique described has an intriguing potential to monitor the progress of scale damge during cooling and complements nicely with other techniques that characterize the mechanical limits of oxide scales. It is recommended that the paper be published in its present form. It is, however, recommended that fig. 11 is described in some more detail as it does not seem to be perfectly clear what the different lines and symbols mean in this figure.

The authors thank the reviewers for these kind words. We also thank the reviewer for the opportunity to improve on Figure 11, the Spallation Map. This has now been completed with improvements with an improved description within the text, all changes have been highlighted in red in the revised manuscript and the caption for Figure 11.

In addition, the acknowledgement has been extended to include the work performed at the NPL where the idea of using IR cameras to detect heat flow from surfaces came from. That would was on thermal barrier coating at room temperature using low temperatures. We were very pleased to find the technique worked for us during cooling.

Highlights

A new technique is presented which monitors and records the local temperature at the surface of a sample during cooling using both an Infra Red and a video camera. The technique is termed: Simultaneous Thermographic and Optical Recording Media Examination (STORME).

Disturbance of the thermal diffusion through the surface oxide from the substrate, due to delamination and spallation, is monitored. For the first time, the radius of the delamination site was measured experimentally at the point of buckle formation and observed during propagation to the point at which spallation of the oxide fragment occurred.

The video recording enabled collection of the spalled fragment for SEM examination to determine the thickness and composition.

The strain energies at each stage in the spallation process of oxides grown on TP347H FG in air-saturated steam at 923 K has been calculated and a Spallation Map constructed.

Simultaneous Thermographic and Optical Recording Media Examination of the First Oxide Spallation Event from the Surface of an Austenitic Stainless Steel

R-L. Mobbs[a,b], J.D. Ramsay[a], T.D. Reynolds[a], S. Gray[c], S.Osgerby[d] and M.P. Taylor[a*]

[a]*The University of Birmingham, Birmingham, B15 2TT, UK*

[b]*Arconic, Kitts Green, Birmingham, B33 9QR.*

[c]*Cranfield University, Bedford, MK43 0AL, UK*

[d]*GE Power, Rugby, CV21 2NH, UK*

[*]*m.p.taylor@bham.ac.uk*

Abstract

Spallation of oxides grown on TP347H FG in air-saturated steam at 923 K for 50 – 1000 hours was investigated using a newly developed technique termed: Simultaneous Thermographic and Optical Recording Media Examination (STORME), recording the temperature disturbance resulting from delamination and spallation, during cooling, using Infra Red and video cameras. For the first time, the radius of the delamination site was measured experimentally at the point of buckle formation and followed during growth to the point of spallation. Collection of the exact spalled fragment was possible. The strain energies at each stage were calculated and a Spallation Map constructed.

Introduction

Spallation of the oxide from the inner surface of the heat exchanger tubing in power plant boilers is of particular importance because this can lead to tube blockages and erosion of the turbine blades further downstream. Blockages of the tube can lead to localised overheating which can eventually lead to rupture. For a better understanding of the spallation process a detailed investigation into the mechanisms leading to loss of oxide fragments is necessary. As the early stages in this process occur at some point during the cooling cycle, interpreting the evidence from ex-situ samples, taken to room temperature, can prove difficult. This can inhibit assessment of the critical factors at the point of delamination and / or spallation.

On exposure to steam-containing environments steels develop a layered surface oxide structure influenced by compositional elements, predominantly chromium [1-13]. At chromium concentrations above 12 wt% a chromium containing oxide develops adjacent to the alloy; below approximately 20 wt% this oxide is a spinel of the generic composition $(Fe,Cr)_3O_4$ and above this value Cr_2O_3 forms; both oxides provide oxidation protection with Cr_2O_3 being more effective than the spinel. Diffusion of iron ions is possible through the spinel oxides which oxidises at the outer surface forming Fe_3O_4. In the alloy of interest in this project a duplex oxide layer consisting of an inwardly growing $(Fe,Cr,Ni)_3O_4$ spinel and an outwardly growing magnetite (Fe_3O_4) layer [1-3, 7, 12]. Under oxygenated steam conditions an outer decoration of haematite (Fe_2O_3) also forms [1, 3-6, 9, 10, 12, 13]. The formation of haematite is often not found in laboratory tests conducted in de-oxygenated steam conditions but is a feature of samples removed from plant and also shown to form under oxygenated steam testing [8-10, 11].

Evidence exists that oxides grown in steam environments are more porous than those grown in dry oxygen or air [1, 9]. Vacancy formation is part of the oxidation process and discussion of their formation and annihilations are given in references, [14-19]. In the case of layered oxides vacancy production can occur at the boundaries between the layers. Coalescence of the vacancies leads to void formation and the development of aligned porosity has been noted for instance within Fe_3O_4 [10] where voids formed close to the site of vacancy formation [14]. This will occur in oxides where there is a divergence in diffusion rates between the cations and anions and has been noted under steam containing environment where enhanced oxygen diffusion rates occur within the scale [16, 17]. Incorporation of the impact of voids on the spallation process has been performed by categorising the features according to geometry, for instance [18].

Spallation of the surface oxide is widely reported [4, 5, 8, 11, 21-23,]. Wright and Dooley reported on the spallation behaviour of the 300 series austenitic stainless steels and demonstrated the loss of the whole outer iron oxide, i.e. haematite and magnetite [4, 21]. In addition to blockage and erosion this also represents loss of oxidation protection. The spallation process results from the stresses generated during cooling due to the large differences in thermal expansion coefficient that can exist between the alloy and oxides [5, 24, 25]. Measurements of the stresses imposed

during cooling show that oxides formed on the inner surface, steam side, of ex-plant tubes made from TP347, were subjected to compressive stresses in the order of several 100 MPa [12].

Techniques such as Acoustic Emission (AE) [22, 26] and dynamic visual observation [23] have been used to detect the temperature range for early cracking within the oxide grown on P92 steel in flowing steam [22] and the temperature at which spallation begins for ferritic and austenitic steels in air, respectively. The stresses within the oxide during cooling have also been measured using in-situ Raman [27] and micro-Raman spectroscopy [28]. Whilst these techniques were somewhat successful in determining key parameters for stress calculations, there have been no reports in the literature imaging samples for the full duration of the cooling stage and recording the temperatures at which changes to the oxide occur. Those techniques also have some limitations with either a lack of imaging or temperature recordings in AE or dynamic visual observation, respectively, as well as limitations as to which oxides are able to be detected in the case of Raman spectroscopy.

In this paper a similar technique to dynamic visual observation [23] has been used but uniquely a thermal imaging Infra Red (IR) camera was employed to identify the temperature at which the delamination and spallation events occurred for individual localised spallation sites. For the first time, the ΔT for localised spallation sites has been obtained along with the radius of the delaminated region. The initial site of spallation was recorded for a series of samples exposed for varying times at 923 K. This approach has been used to study the spallation behaviour of oxides grown under steam on fine-grained (FG) austenitic stainless steel TP347H FG, where TP is Tube Piping; used as superheater and reheater tubing in biomass and coal fired power plants. A detailed examination of the spalled oxide particles was conducted using Scanning Electron Microscopy (SEM). Cross-sectional examination of bulk specimens was conducted to aid interpretation of the findings. Interpretation of the data will be conducted in line with the theoretical approach presented in reference [24].

Experimental Procedure

Isothermal oxidation in air saturated steam was carried out at atmospheric pressure on TP347H FG (fine grained) austenitic stainless steel, with a grain size of 20 μm and the composition shown in Table 1. Samples were extracted from tubes, as used in

plant, with an internal diameter of 28 mm and a wall thickness of 4.5 mm. The inner surface of the tube was pickled according to usual industrial practice. A silicon carbide cutting disc was used to make 10 mm sections of the tube which were subsequently cut into 60° arcs, Figure 1; producing six samples from each section. All samples were cleaned in ethanol prior to exposure in the steam oxidation rigs, shown in Figure 2.

Deionised water was pumped into two barrels, A and B, pressurised to approximately 0.5 bar, using air to achieve the air saturated steam environment. A dosing pump transferred the water from the barrels to the work tube where, on entry, it evaporated and travelled through the tube to the exit port where it condensed, ensuring unidirectional flow of steam. The furnace temperature was set to 923 K for all tests presented here. Weighing scales were used to monitor the capacity of the water barrels during testing. The rig was designed to allow independent filling and emptying of the water barrels ensuring a continuous flow of water to the work tube. The steam flow was set up and monitored prior to testing. Once flow was stable, samples were placed on alumina boats and inserted via the exit port, which was then sealed. At the end of the exposure period samples were removed from the hot furnace and cooled in laboratory air.

Previous studies have shown that spallation does not occur in closely controlled deoxygenated steam conditions [29], but does occur in plant conditions [5]. For this reason, air saturated steam with a partial pressure of oxygen of approximately 1×10^{-5} has been used in this work to enable a study of the spallation effects comparable to those seen in plant, [5, 21].

The thermal behaviour of the samples during cooling was monitored using Simultaneous Thermographic and Optical Recording Media Examination (STORME). This included a Microepsilon TIM400 thermal imaging camera and a video camera. The technique monitored the impact of the formation of subsurface delamination interfaces and buckling, etc., on the disruption of heat transferred from the substrate alloy to the surface. IR emissions from the surface recorded the temperature, using an emissivity value of 0.89. The temperature recorded by the IR camera was confirmed using a calibrated R-type thermocouple adjacent to a sample.

To perfect the data collection using STORME, a number of positional configurations of the sample relative to the cameras were investigated. The optimum configuration

was found to be removal of the samples from the hot alumina boats and positioning on a heat-proof surface with the concave surface facing both cameras at the same level. In this way the heat emanating from the sample only, and not the alumina furnace boat, was recorded and any spalled oxide fragment falling from the surface could be located for collection and further examination.

Synchronisation of the thermal imaging camera with a video camera enabled determination of the precise site, time and temperature at which localised spallation occurred. The site of spallation was identified on both cameras and the IR images were used to trace backwards in time, tracking the changes in thermal contours at the site. In this way it was possible to identify the delamination event within the oxide layer that lead to spallation as, buckle formation, characterised by a region of decohesion due to the oxide having expanded outwards, leads to the sudden, local decrease in temperature. At this point the heat transfer through the oxide would be interrupted decreasing the temperature recorded at the outer surface. The temperature of the region at the point of delamination was recorded. In addition, the temperature at the site when spallation occurred was also recorded and the ΔT for each event was calculated.

The oxide fragment that had spalled from that area was located using the video recording, and collected using magnetic tweezers. These were meticulously positioned on carbon adhesive tape mounted on aluminium stubs, enabling examination of the cross-section using a JEOL 7000 FEG Scanning Electron Microscope (SEM). Examination of spall fragments and the surface of samples post steam oxidation was also carried out using a FEI Quanta 3D FIB-SEM with Energy Dispersive X-ray Spectroscopy (EDS) facilities attached. Approximately 20 oxide thickness measurements were taken from the SEM images for each fragment.

For cross-sectional analysis, samples were mounted in epoxy resin and ground using SiC papers from 240 to 1200 grit. These were polished using diamond suspension and finished using OPA-sol. SEM with EDS and Wavelength Dispersive X-ray Spectroscopy (EDS/WDS) capabilities were used to examine the oxide formed on the inner, pickled surface, i.e., steam side, of the tubing.

Results

STORME

As described in the experimental procedure the STORME technique first identifies the site of the first spallation event using a video camera. The IR camera images were traced backwards in time observing changes in the thermal contours on the surface. A series of low resolution images demonstrating the information provided by the STORME technique, in chronological order starting from just prior to delamination and buckle formation, are shown in Figure 3. Figure 3 (a) is an IR snapshot during cooling prior to any delamination or spallation events, showing that the heat loss was greatest from the edges of the sample and a slight temperature gradient of 21 K developed across the sample from top to bottom due to contact with the cold, heat resistance surface. Figure 3 (b) shows the IR image of the surface one second later than (a) where the thermal profile indicated a highly localised temperature decrease occurring at the subsequent spallation site, circled. Figure 3 (c) shows the IR image at the point where spallation of a fragment from that site occurred, also showing a rapid, localised change in temperature. Figure 3 (d) is the video snapshot of the surface at the point of spallation, at the same time interval as (c). This image was also used to identify the location of the spalled fragment in front of the sample for collection and examination.

Using higher resolution IR images the radius of the site, from the time of delamination to the time of spallation, was measured at 5 second intervals and plotted as a function of the temperature drop from 923 K, Figure 4. This showed for this example, that after the initial delamination event, with a radius of approximately 0.37 mm, the buckled region was stable for approximately 20 seconds, or a change in temperature of 43 K. The horizontal line included in the plot demonstrates the point at which the radius increased and the buckle began to grow. For the purpose of this exercise the data for the beginning of the propagation stage is taken as the point at which the radius was detected to grow, 0.38 mm, with the corresponding temperature drop of 330 K. The buckle continued to grow until, at approximately 0.44 mm and a temperature drop of 395 K, the oxide fragment spalled; vertical line. This sequence was observed in all samples.

The radii of the first delaminated sites and the temperature drops from 923 K at which delamination, propagation and spallation occurred, ΔT_{del}, ΔT_{prop} and ΔT_{sp}, respectively, are recorded in Table 2. As the samples continued to cool, further

spallation events took place across the surface of the samples with significant loss of the outer oxide in some cases; the amount of spallation increased with thermal exposure.

Cross-Sectional Analysis

Cross-sections through the samples enabled analysis of the composition of the oxides formed on the surface of samples, Figure 5. This revealed the expected sequence of layers from the alloy outwards of: iron / nickel / chromium spinel, Fe_3O_4 (magnetite) overlaid by Fe_2O_3 (haematite). A series of cross-sections through the samples revealed the development of the oxides showing evidence of void formation, cracking and regions where spallation had occurred; the number and size of each increased with increasing exposure time, Figure 6. For the shorter-term tests, images of sites where limited spallation of the outer oxide had occurred have been selected, Figures 6 (a - c). These show a dense Fe_2O_3 outer layer and that the majority of the voids were located within the underlying Fe_3O_4 layer. The presence of a significant and stable buckle, Figure 6 (b), showed that delamination occurred at the Fe_2O_3 / Fe_3O_4 interface. The thickness of the outer dense layer in Figure 6 (b) was approximately 5 μm. Also, in Figure 6 (b), there is evidence that lateral growth of buckles had occurred, as observed from the IR camera images using the STORME technique and shown in Figure 4.

At longer times Figure 6 (d – f), significant spallation of the oxide from the surface of the samples occurred during cooling. Remnants of the walls of the voids were obvious at the remaining outer surface of the oxide, demonstrating that an interface of aligned voids developed within the oxide while at temperature. This interface was observed to be at the spinel / Fe_3O_4 boundary in some regions, Figure 6 (d and e), and wholly within the magnetite in others, Figure 6 (f). The early formation of such an interface with increased alignment of voids can be seen in Figure 6 (c). Fine cracks within the oxide layers were also seen running roughly parallel to the alloy surface.

Spalled Oxide Fragments

The angle of the video camera to the samples enabled the recovery of the primary spalled fragments for detailed examination under SEM, Figure 7. This revealed that, for 50 and 100 hour exposures the fragment consisted of one oxide morphology,

Figure 7 (a), however, at 300 hours and longer exposure times two morphologies were observed, Figure 7 (b). The difference between the two morphologies corresponded to the two types of iron-oxide formed, Fe_2O_3 and Fe_3O_4. No spinel was observed in these fragments. The difference in morphology was sufficient to identify the oxides present in the spalled fragments and to measure the respective thicknesses, Table 2. Plotting this data, Figure 8, showed that the total thickness of the spalled fragments increased with increasing exposure time. The mean thickness of the fragment collected after 50 hours exposure was 5.5 μm, similar to the thickness of the buckled region in Figure 6 (a), this compliments the observation made for the spalled fragments after 50 and 100 hours thermal exposure that spallation of only the Fe_2O_3 layer had occurred and that the delamination at these times was at the interface with the Fe_3O_4.

Figure 8 shows that the Fe_2O_3 layer composing the fragments increased only slightly in thickness over the complete testing period. At exposure times longer than 100 hours the thickness of the spalled fragments was due mainly to the increasing contribution of Fe_3O_4 to the layer.

Analysis of Data

Driving Force for Spallation

The oxides formed under isothermal exposure can be assumed to be relatively stress-free at temperature. Thus, the strain, $\boldsymbol{\varepsilon}$, induced within the oxide on cooling can be determined by [25]:

$$\varepsilon = \Delta\alpha.\Delta T \qquad (1)$$

where $\Delta\alpha$ is the difference in the thermal expansion coefficients between the alloy and the oxide in K^{-1}, ΔT is the temperature change in K. Similarly, the strain energy within the surface oxide, relative to the much thicker substrate alloy, W^*, can be described by [24, 30]:

$$W^* = (\Delta\alpha)^2(\Delta T)^2(1-\nu_{ox})E_{ox}\xi \qquad (2)$$

where $\Delta\alpha$ and ΔT are as given above, ν_{ox} is the Poisson's ratio of the oxide, E_{ox} is the Young's modulus of the oxide in Pa, and ξ is the thickness of the oxide in m. The

driving force for spallation is the release of this strain energy by overcoming interfacial adhesion.

The mechanism through which spallation occurs has been considered previously by H.E. Evans *et al*. [31] and buckling considered by A.G. Evans and J.W. Hutchinson [32] and C.H. Wells *et al*. [33]. These mechanisms can be modelled by:

$$\Delta T_W = \left(\frac{\gamma_F}{\xi E_{ox}(\Delta\alpha)^2(1-\nu_{ox})}\right)^{1/2} \quad (3)$$

and:

$$\Delta T_b = \frac{1.22}{\Delta\alpha(1-\nu_{ox}{}^2)}\left(\frac{\xi}{R}\right)^2 \quad (4)$$

where ΔT_w and ΔT_b are the temperature drops, in K, to initiate spallation via strain energy release or by buckle formation, respectively, γ_F is fracture energy in J.m^{-2}, R is the radius of decohesion in m, and all other parameters are as given above.

In some cases, buckling does not result in spallation, i.e., stable buckles form. Propagation of the buckle by extension of a crack along the interface may occur on further cooling, leading to spallation of the oxide. This is termed unstable buckling, and can be described by the following condition [33]:

$$\Delta T_{ub} = \left(\frac{1.052\xi^4}{R^4} + \frac{1.041\gamma_F}{E_{ox}\xi}\right)^{1/2} . \frac{1}{\Delta\alpha} \quad (5)$$

where ΔT_{ub} is the critical temperature drop in K, required to initiate spallation via unstable buckling and all other parameters are as above.

Equation 5 includes a term corresponding to the initiation of the buckle, i.e., Equation 4, and a term corresponding to the propagation of the buckle. This inclusion indicates the necessity for the prior formation of a buckle. The buckled area of decohesion grows when the release in strain energy is sufficient to overcome the interfacial energy.

Values for the Young's modulus of the oxides are reported in the literature as 230 and 210 GPa for Fe_2O_3 and Fe_3O_4, respectively, [34, 35]. The Poisson's ratios for each oxide, respectively, are 0.19 and 0.29 [25]. The choice of the values for the coefficient of thermal expansion, α, needs careful consideration. A paper by G. Holcomb [36] clarifies the differences in the techniques used to determine this value, a summary is

provided in Appendix A. Also included in Appendix A are the thermal expansion coefficients, α, for Fe_2O_3, Fe_3O_4, and TP347H over the temperature range of relevance to this study, Figure A1. The α's and calculated $\Delta\alpha$'s at each ΔT obtained from the STORME technique, i.e., ΔT_{del}, ΔT_{prop} and ΔT_{spall}, are presented in Tables A1, A2 and A3, respectively. These data along with the dimensions and ΔTs, Table 2, will be used in the analysis presented in the next sections. The spallation process occurring in this study included only the iron oxides and no spinel was observed in the spalled fragments. In addition, cross-sectional examination showed minimal cracking in the spinel. Thus, for the purpose of the analysis conducted here only the iron oxides will be considered.

Delamination and Buckle Formation

The strain and strain energy within the buckled oxide at the point of formation, for each thermal exposure, was calculated using Equations 1 and 2, respectively, Table 3. The strain values in the Fe_3O_4 are slightly lower than that in the Fe_2O_3 and both fall within the elastic range of both oxides for all thermal exposures [25]. An additional calculation included in Table 3, the stress in both oxides at the point of buckle formation based on the strain, showed that a compressive stress was induced in the oxide the values in the range of 378-683 MPa. This is consistent with that measured using XRD on the oxides formed on the steam side of ex-situ heat exchange tubes made of TP347H, [11], contrasting to the tensile stresses recorded for similar oxides formed on ferritic alloys.

The strain energy values, necessary to overcome the adhesion at the Fe_2O_3 / Fe_3O_4 interface, obtained from the 50 and 100 hours exposure times, was relatively constant at 6.7 J mol^{-1}, Table 3. The calculated strain energy values at longer exposures, up to 750 hours, showed an initial increase followed by a general decrease within the Fe_2O_3 layer and a lower but increasing value for the Fe_3O_4 layer. A large increase in strain energy was observed in the 1000 hours exposure sample in both oxide layers although the strain within each oxide were within the elastic region of maps proposed in reference 25, with the value determined in the Fe_3O_4 close to the brittle behaviour or spallation boundary. The value for the total thickness shows a general increase with increasing thermal exposure.

It has been demonstrated in this study that once formed the buckle showed a period of stability, Figure 4 and Table 2. To study the formation in more detail the delamination STORME data, Table A1 were applied to Equation 4, the condition for stable buckle formation. In this equation the term ξ / R reflects the relationship between the thickness of the oxide layer and radius of the delaminated region. It is known that a larger area of decohesion, with a radius up to 50 times greater compared to the thickness of oxide, is necessary to enable buckle formation [24]. Figure 9 is a plot of the radius at the point of delamination against the oxide thickness of spalled oxide fragments, Table 2. For mixed oxide fragments, the radius is plotted against the total thickness, x symbols, and the thickness of Fe_2O_3 within that fragment, + symbols. Fragments that consist entirely of Fe_2O_3 are indicated by ✳. A number of dashed lines are included in the plot to indicate ξ / R ratios of 1:50, 1:40, 1:30, 1:20 and 1:10. After 50 and 100 hours exposure, where Fe_2O_3 was the only component of the oxide fragment, the ξ / R ratios were 1:42 and 1:32, respectively, fitting well with the theory. When considering the total oxide thickness, x symbols, the ξ / R ratios continue to follow the 1:30 trend but abruptly change to the 1:10 ratio at 750 hours exposure. This confirms the need for a large area of decohesion to be present to enable buckling of the overlying oxide layers.

Examination of the strain energies, Table 3, show that at 350 and 500 hours the values in the Fe_3O_4 are lower by half, than that in the Fe_2O_3 thus it can be envisaged that the strain within the latter is the driving force for buckle formation. Taking this approach and plotting the measured R values against the Fe_2O_3 thickness, + symbols in Figure 9, does show greater agreement with the theoretical values for all samples included. A similar effect was seen for the samples exposed for longer durations. This suggests that in subsequent calculations, where oxide thickness measurements are required, it is the value obtained from the Fe_2O_3 layer that is the appropriate value to be used. The necessity of the presence of Fe_2O_3 to initiate spallation was confirmed by previous data obtained using the rigs in this study where deoxygenated water was used [13]. In that work, where no Fe_2O_3 was present no spallation was observed.

Propagation of Buckle to Spallation

To evaluate the propagation stage, data from Table 2 and Table A2 were input into Equation 5 to obtain the fracture energy, γ_F, necessary for crack growth from the edge

of the buckle along that interface, Table 4. The driving force for stress development in this system is the difference in the α between the metal substrate and the oxide. Thus, two sets of calculations are presented in Table 4 containing the values based on measurements for Fe_2O_3 and Fe_3O_4 compared independently to the alloy.

The data available for the two lowest exposure times were relatively easy to interpret as it has been established that the spalled oxide fragment consisted of only Fe_2O_3, Figure 6 (b) and Figure 7 (a). A value of 8.3 J m^{-2} was calculated for the fracture energy of the Fe_2O_3 / Fe_3O_4 interface.

The fracture energy for a crack propagating through the Fe_3O_4 was a little more difficult to interpret as the internal interface consisted of aligned voids developed during thermal exposure with some variability in the location within the layer. To understand the effects of each oxide present, the contributions are considered separately. Taking first the effect of the Fe_2O_3 contribution, an increase in fracture energy was observed up to 500 hours exposure, this was followed by a decrease at 750 hours and a large increase at 1000 hours, Table 4. However, the values based on data for Fe_3O_4 showed lower values and indicated a weaker interface up to 750 hours exposure. The calculated strains at the point of propagation were slightly lower compared to the short-term exposures again, indicating the development of a weakness within the oxides. The values obtained for the 1000 hours sample were noticeably higher than those for the shorter exposure times. This might represent the influence of the thicker oxide above the relatively small delaminated region, inhibiting crack opening and thus generating lower tensile stresses at the edge of the buckle. It might also suggest that strain release mechanisms such as micro-cracking, and buckle formation have occurred. The higher calculated strain values for these samples would support either of these two theories.

The increase in the radii of the buckles from formation to spallation, ΔR, for each sample, from shortest thermal exposure to longest, were 0.22, 0.25, 0.23, 0.07, 0.18 and 0.16 mm. The ΔR values were relatively uniform at approximately 0.2 mm except for the 500 hours exposure. During this stage the crack may extend to the surface or it may intersect with another crack or defect in the oxide emerging at the surface. Examination of the spalled fragments, Figure 7, suggested that the horizontal delamination cracks intersected a near vertical crack to enable spallation. As shown

in the 500 hour exposure, the distance to intersection can be very short, however, the other samples showed a level of consistency in the growth length to the final radius at the point of spallation, which was between 0.37 and 0.53 mm. An explanation may be that deformation of the oxide at these low temperatures results in the formation of localised tensile stresses at the underside of the edges of the buckle leading to the formation of a vertical crack.

Table 5 gives the calculations of the strain in each oxide, Eq. 1, and the strain energy, Eq. 2, at the point of spallation for all samples. The strain values fall within the brittle failure or spallation regime for both iron oxides, as defined in reference 26, although there is a level of variability in the values. An average value of the strain energy in the two shortest exposure times was 16.8 J mol^{-1}. This value increased to 23 J mol^{-1} at longer exposures when considering the Fe_2O_3 layer in relation to the alloy. A general increase was observed in the strain energies when considering Fe_3O_4 eventually exceeding the values calculated for the Fe_2O_3 layer. When considering the total oxide thickness the strain energy values showed a general increase with increasing exposure time. The level of variability of the values associated with the final spallation event represent the different factors at play, e.g. influence of oxide thickness, formation of decohesion region, but primarily the intersection of multiple cracks to release the fragment.

Discussion

This study has demonstrated the ability of the technique termed STORME to obtaining information on the primary spallation site at the point of initial buckle formation, propagation and final loss. Schematic diagrams describing the findings are present in Figure 10.

For the short term exposures spallation was characterised by delamination at the Fe_2O_3 / Fe_3O_4 interface. The strain energy of formation of the initial buckle was found to be 6.7 J mol^{-1}. Analysis of the data showed that the ratio of the thickness of the spalled oxide fragments to the initial radius of decohesion was 1:42 and 1:32 following 50 and 100 hours exposure, respectively. This is in keeping with the theory on buckle formation whereby a large area of decohesion, relative to the thickness of the overlying oxide, is necessary for buckling to occur. Immediately after formation a period of stability of the buckles was noted before propagation began on further cooling, with a

ΔT from buckle formation to propagation of 18 and 28 K for the 50 and 100 hour exposures, respectively. The fracture energy of the Fe_2O_3 / Fe_3O_4 interface was calculated as 8.3 J m^{-2} and the radius of the buckled area increased by approximately 0.23 mm before intersecting with the surface resulting in spallation of the oxide fragment. At the point of spallation, a strain energy of approximately 16.8 J mol^{-1} was calculated.

With increasing exposure times, the spalled oxide fragments were composed of Fe_2O_3 with an increasing thickness of Fe_3O_4. At the point of delamination the calculated strains in each oxide were slightly lower than that for the shorter exposure times up to 1000 hours where the values increased slightly. At this stage in the process the values were within the elastic behaviour limits of both iron oxides [26]. Fluctuations were seen in the calculated strain energy values in the Fe_2O_3 layer. Whereas, in the Fe_3O_4 layer a lower strain energy was calculated at 300 hours exposure which increased with increasing time and increasing layer thickness. Analysis of the data suggested that the Fe_2O_3 layer was the driving force for buckle formation as the thickness to radius ratio more closely correlated to the theoretical values. When considering the total oxide thickness the ξ / R ratio followed the 1:30 ratio for the 300 and 500 hour exposures and transferred close to the 1:10 ratio after 750 hours. It was concluded that the thickness of the Fe_2O_3 layer was a significant parameter in driving the delamination process. It was noted in other work performed on the same rigs that, under de-oxygenated steam Fe_2O_3 did not form and no spallation was recorded [13]. When considering the whole system reported here the calculated strain energies at the point of buckle formation indicated the development of an interface of lower adhesion strength developing within the Fe_3O_4 layer. This was linked to the coalescence of vacancies into voids formed as a consequence of the oxidation process at the Fe_3O_4 / $(Fe,Cr,Ni)_3O_4$ boundary. The continued growth of the Fe_3O_4 above this interface resulted in the observed increase in the thickness of the spalled fragments.

For the next stage, propagation, two calculations were performed treating the two oxides separately. This showed that the fracture energy needed to overcome the adhesion strength of the spalling interface was lower than the value of 8.3 J m^{-2} calculated for the Fe_2O_3 / Fe_3O_4 interface, in samples exposed up to 750 hours. This demonstrated that, with increasing exposure time an interface with a lower fracture

toughness was developing within the Fe_3O_4 layer. Cross-sectional examination showed increased levels of void formation with increased exposure time in the Fe_3O_4 which was not noted in the Fe_2O_3 layer which remained dense, Figure 6. There was also evidence in the micrographs that a level of void alignment was occurring. This agrees well with the established growth mechanisms for Fe_3O_4 type oxides, presented earlier, where vacancies are generated at the spinel interface especially under steam oxidation conditions. Diffusion and coalescence of these vacancies would lead to the development of voids in an aligned configuration resulting in a localised decrease in fracture toughness. Models have been developed to attribute numerical terms to the various aspects of voids such as geometry and alignment [18].

The strain energy for delamination, Table 3, and the fracture energies for propagation, Table 4, determined for the 1000 hours exposure showed a marked increase in values. This may represent the higher strains necessary to deform the thicker buckled oxide layer, also shown in the Tables. It may demonstrate that some level of stress relief may have occurred, e.g. micro-cracking.

A Spallation Map of ΔT for delamination, propagation and spallation events against Fe_2O_3 thickness has been constructed for the alloy oxide system investigated in this study, Figure 11. Also plotted is the boundary based on the strain energy criterion given in Equation 3 using the materials properties for Fe_2O_3: E_{ox} = 230 GPa, v = 0.19. For simplicity a value for $\Delta\alpha$ = 7 x 10^{-6} K^{-1} was used, closely matching the values determined in this study, Appendix A, and to demonstrate the effect of the fracture energy plots using values of 3, 5, 7 or 9 $Jmol^{-1}$ are shown, as indicated in Figure 11. The data follows the trend described in Equation 3 using a fracture energy of 7 $Jmol^{-1}$ for initial buckling event and thus this forms a boundary condition for the oxide alloy system up to a thickness of Fe_2O_3 of 7.5 μm or exposure duration of 750 hours. A change in behaviour is seen in the sample exposed for 1000 hour in steam. At this point the data appears to follow the established buckling behaviour, Equation 4, where the (ξ/R) term plays a significant influence on the strain necessary to deform the oxide above a delaminated region into a buckle. Plots of Equation 4 using ξ/R values of 0.04 and 0.047 are also included in the Figure 11 to indicate the point at which the change in mechanism occurs.

The new technique termed STORME has provided critical details of a variety of parameters for the first spallation site in the austenitic steel, TP347H FG. Analysis of the data has shown that the spallation behaviour follows the strain energy criterion [31] up to 750 hours or a Fe_2O_3 thickness of 7.5 μm. A change in mechanism was shown at 1000 hours exposure or 8 μm where the behaviour follows the established buckling mechanism [32, 33]. The data showed that at the point of delamination the strain within the oxides was within the elastic regime of the oxides and that this increased, with further temperature decrease at the point of spallation, to the brittle boundary. Analysis of strain energies, specific to each spallation site, provided values for the energies to delaminate the Fe_2O_3 / Fe_3O_4 interface and demonstrated the effect of the development of a weakened interface within the Fe_3O_4, formed due to the production of voids aligned at or close to the interface with the spinel layer. Fracture energies at the point of propagation were also calculated for the two interfaces. The data collected also showed that the compressive stress developed in the oxides were similar to that measured in reference 11.

Some sample-to-sample variability was observed as well as in the strain energies at the point of spallation. The fluctuations in the latter could be attributed to strain release mechanisms such as micro-cracking and interaction between cracks and voids. Examination of the cross-sections of all samples did show increasing levels of cracking and void formation within the Fe_3O_4 layer with time. The level of cracking indicated accommodation of strain induced during cooling by a series of stress relief events. Defects within the Fe_3O_4, e.g. voids or grain boundaries, could act as sites of crack initiation. The voids might also interact with the progression of cracks, i.e., a void in the path of a crack may arrest the progression by blunting the crack tip due to the geometry effects.

It should be remembered that the level of cracking observed in the cross-sections does not represent that present at the point of delamination and buckle formation that occurred at a higher temperature. On continued cooling significant levels of spallation and cracking of the surface oxide were observed. This highlights the advantages of the STORME technique over ex-situ examination of samples. The data collected using this in-situ technique includes the radius of the buckle at the point of formation and the temperature drop at that event. The technique also enabled the collection of the exact oxide fragment to determine the thickness.

Conclusion

A technique, termed STORME, has been developed capable of detecting critical data at the point of formation and growth of delaminated regions within the surface iron oxides formed on the austenitic steel TP347 FG. Using the STORME technique it has been possible to obtain unique site specific data on the primary spallation event from the surface of an alloy exposed to an oxidising steam environment. The alignment of the cameras to the sample face enabled identification and thus collection of the spalled oxide fragment for examination and measurement of the thickness, and identification of the composition.

The data collected has shown that, in the very early stages the difference in the thermal contraction between the Fe_2O_3 layer and the alloy is the driving force for spallation of oxide fragments. The difference was greater than that generated in the Fe_3O_4 layer. In the shortest exposure tests it was possible to determine the strain at the point of delamination at the Fe_2O_3 / Fe_3O_4 interface, to measure the radius of the buckle formed and thus determine the energy of adhesion and estimate the fracture energy needed for buckle extension as the system continued to cool.

With increasing exposure time it was found that an interface developed within the Fe_3O_4 layer with a lower fracture energy than the Fe_2O_3 / Fe_3O_4 interface. This was attributed to the mechanisms of growth of Fe_3O_4 and the coalescence of the vacancies generated in this process, producing aligned voids at or close to the interface with the underlying spinel layer. The growth of the buckled region was monitored until spallation of the oxide fragment occurred; the fracture energy was shown to be lower than that along the Fe_2O_3 / Fe_3O_4 interface.

In all cases the region of delamination resulting in the initial buckle matched the theoretical estimates based on the thickness of the Fe_2O_3 layer. It was found that by plotting events on a spallation map, Figure 11, the data fit well to a strain energy release to form the buckle of approximately 7 J mol^{-1}. At the longest exposure time included in the study a higher strain energy was determined. This was attributed to the additional strain needed to deform the thicker oxide above a region of delamination, well below the theoretical value. At this point the data fitted well to the Wells and Evans model for buckle formation described by Equation 4.

Acknowledgements

The completion of this manuscript was possible due to the significant contribution made by Professor Hugh Evans to this field of research. Although he was the principle supervisor for this work he was not able to complete the final analysis of the data; any errors in concept rest entirely with the authors. It was a privilege for each of the authors to know and be guided by him.

The authors would also like to thank the UK Engineering and Physical Science Research Council (EPSRC) and BF2RA for financial support for this work. Funding for this work is also provided as part of the Efficient Fossil Energy Technologies (EFET) doctorate centre. The Centre of Electron Microscopy (CEM) at the University of Birmingham is also acknowledged for their support. In addition, the inspiration for the STORME technique came from work conducted at the National Physical Laboratory, NPL, UK, using the interruption to heat flow through thermal barrier coatings to detect internal cracks and sites of delamination.

References

[1] S.R. Saunders, M. Monteiro, F. Rizzo, The oxidation behaviour of metals and alloys at high temperatures in atmospheres containing water vapour: A Review, Progress in Mat Sci. 53 (2008) 775-837.

[2] A.N. Hansson, K. Pantleon, F.B. Grumsen, M.A. Somers, Microstructure evolution during steam oxidation of a Nb stabilised austenitic stainless steel, Oxid. Metals 73 (2010) 289-309.

[3] A.T. Fry, S. Osgerby, M. Wright, Oxidation of alloys in steam Environments - A Review, NPL Report MATC(A) (2002) 90.

[4] I. G. Wright, R. B. Dooley, A review of the oxidation behaviour of structural alloys in steam, Inter. Mat .Rev. 55, (2010) 129-167.

[5] J. Armitt, R. Holmes, M. I. Manning, D. B. Meadowcroft, E. Metcalfe, The spalling of steam-grown oxide from superheater and reheater tube steels, EPRI report FP-686, Palo Alto, (1978).

[6] A.N. Hansson, H. Danielsen, F.B. Grumse, M. Montgomery, Microstructural investigation of the oxide formed on TP347H FG during long-term steam oxidation, Mater. Corros. 61 (2010) 665-675.

[7] N.J. Simms, P.J. Kilgallon, J.E. Oakey, Degradation of heat exchanger materials under biomass co-firing conditions, Mater. High Temp. 24 (2014) 333-342.

[8] R.B. Dooley, Program on technology innovation: oxide growth and exfoliation on alloys exposed to steam, EPRI. (2007).

[9] N.K. Othman, J. Zhang, D.J. Young, Water vapour effects on Fe-Cr alloy oxidation, Oxid. Metals 73 (2019) 337-352.

[10] D.M. Gorman, A.T. Fry, The early morphological development of the near surface region of pickled grade 91 tubing exposed to steam and its long term implications, Metals 6 (2016) 62-78.

[11] K. Pantelon and M. Montgomery, Phase identification and internal stress analysis of steamside oxides on plant exposed superheater tubes, Metal. Mater. Trans. A 43A, (2012) 1477-1486.

[12] T. Dudziak, M. Lukaszewicz, N. Simms, J. R. Nicholls, Steam oxidation of TP347H FG, Super 304H and HR3C - analysis of significance of steam flowrate and specimen surface finish, Corros. Eng., Sci. Tech. 50, (2015) 272-282.

[13] J. C. Rosser, M. I. Bass, C. Cooper, T. Lant, P. D. Brown, B. J. Connolly, H. E. Evans, Steam oxidation of Super 304H and shot-peened Super 304H, Mater. High Temp. 29 (2012) 95-106.

[14] M.Michalik, M. Hansel, J. Zurek, L. Singhheiser, W.J. Quadakkers, Steam oxidation of ferritic steels – laboratory test kinetics data, Mater. High Temp. 22 (2005) 47-60.

[15] H.E. Evans, Spallation of oxide from stainless steel AGR nuclear fuel cladding: mechanisms and consequences, Mater. Sci. Tech, 4 (1988) 414-420.

[16] T. Maruyama, N. Fukagai, M. Uedu, K. Kawamura, Chemical potential deistribution and void formation in magnetite scale formed in oxidation of iron at 823 K,Mater. Sci. Forum 461-464 (2004), 807.

[17] M. Ueda, K. Kawamura, T. Maruyama, Void formation in magnetite scale formed on iron at 823 K – Elucidation by chemical potential distribution, Mater. Sci. Forum 522-523 (2006), 37-44

[18] M. Schutze, P.F. Tortorelli. I.G. Wright, Development of a compressive oxide scale failure diagram, Oxid. of Metals 73 (2010) 389-418.

[19] Richard P. Oleksak, Monica Kapoor, Daniel. E. Perea, Gordon R. Holcomb, Ömer N. Doğan, The role of metal vacancies during high-temperature oxidation of alloys, Mater. Degradation. 25 (2018) 1-8.

[20] A. Atkinson, Transport processes during the growth of oxide films at elevated temperature, Review of Modern Phys. 57 (1985) 437-470.

[21] I. G. Wright, R. B. Dooley, Morphologies of oxide growth and exfoliation in superheater and reheater tubing of steam boilers, Mater. High Temp. 28 (2011) 40-57.

[22] S. Osgerby, Oxide Scale Damage and Spallation in P92 Martensitic Steel, Mater. High Temp.17 (2000) 307-310.

[23] A. Hayashi, N. Hiraide, Y. Inoue, Spallation behaviour of oxide scale on stainless steels, Oxid. of Metals. 85 (2016) 87-101.

[24] H.E. Evans, Stress effects in high temperature oxidation of metals, Inter. Mater. Reviews, 40 (1995), 1-40.

[25] J. Robertson, M.I. Manning, Limits to adherence of oxide scales, Mater. Sci. Tech. 6 (1990) 81-91.

[26] M. M. Nagl, W. T. Evans, S. R. Saunders, D. J. Hall, Investigation of failure of brittle layers under compressive stresses using acoustic emission, Mater. Sci. and Tech. 8 (1992) 1043-1049.

[27] A. Galerie, F. Toscan, M. Dupeux, J. Mougin, G. Lucazeau, C. Valot, A.-M. Huntz, L. Antoni, Stress and adhesion of chromia rich scales on ferritic stainless steels in relation with spallation, Mater. Research. 7, (2004) 81-88.

[28] M. Guerain, P. Goudeau, B. Panicaud, J. Grosseau-Poussard, Local stress determination in chromia-former thanks to micro-Raman spectroscopy: A way to

investigate spontaneous delamination processes, J. Applied Phys. 113 (2013) 063502-1 – 063502-7.

[29] M. Lukaszewicz, N. J. Simms, T. Dudziak, J. R. Nicholls, Effect of steam flow rate and sample orientation on steam oxidation of ferritic and austenitic steels at 650 and 700°C, Oxid. of Metals 79, (2013) 473-483.

[30] H. E. Evans, Spallation models and their relevance to steam-grown oxides, Mater. High Temp. 22 (2005) 155-166.

[31] H. E. Evans, R. C. Lobb, Conditions for the initiation of oxide-scale cracking and spallation, Corros. Sci. 24 (1984) 209-222.

[32] A. G. Evans, J. W. Hutchinson, On the mechanics of delamination and spalling in compressed films, *Inter. J. Solids Structures,* 20 (1984) 455-466.

[33] C. H. Wells, P. S. Follansbee, R. R. Dils, Stress effects and the oxidation of metals, New York: AIME, (1975).

[34] D. Chicot, J. Mendoza, A. Zaoui, G. Louis, V. Lepingle, F. Roudet, J. Lesage, Mechanical properties of Magnetite (Fe_3O_4), Haematite (alpha-Fe_2O_3) and Geothite (alpha-FeO.OH) by instrumental indentation and Molecular Dynamics Analysis, Mater. Chem. Phys. 129 (2011) 862-870.

[35] V. Panjkovic, Friction and the hot rolling of steel, New York: CRC Press, (2014).

[36] G. R. Holcomb, A Review of the thermal expansion of magnetite, Mater. High Temp. 36 (2019) 232-239.

APPENDIX A

The coefficient of thermal expansion, α, of materials can be described either as a *true* value:-

$$\alpha_T = \frac{dx(T)}{x(T)dT} \qquad \text{(A1)}$$

or a *mean* value:-

$$\alpha_M = \frac{x(T)-x(T^o)}{x(T^o)(T-T^o)} \qquad \text{(A2)}$$

where x(T) is the sample length at the test temperature and x(T^o) is the length at a reference temperature.

The differences in these two approaches are discussed in detail in reference 1, where it is stated that α_M is of relevance to the analysis of spallation. The values of α_M for magnetite will be taken from that evaluation [1]. A fifth-order polynomial fit was deduced for the available data, Equation A3:

$$\alpha_M = 8.007 \times 10^{-20}T^5 - 1.995 \times 10^{-16}T^4 + 1.591 \times 10^{-13}T^3 - 5.038 \times 10^{-11}T^2 + 1.604 \times 10^{-8}T + 7.275 \times 10^{-6} \pm 1.311 \times 10^{-6} \ (R^2 = 0.71) \qquad \text{(A3)}$$

where T is temperature in K.

That evaluation used data from Takeda [2] for Fe_3O_4 and thus for consistence in the analysis conducted in this work, Takeda's values for Fe_2O_3, determined in the same manner, will also be used [2]. The relevant thermal expansion data are plotted in Figure A1 along with comparable α_M data for the alloy used here, TP347H.[3].

The polynomial fit to the α_M data for Fe_2O_3 from reference A2 is:

$$\alpha_M = 7.051 \times 10^{-20}T^5 - 2.935 \times 10^{-16}T^4 + 4.632 \times 10^{-13}T^3 - 3.490 \times 10^{-10}T^2 + 1.322 \times 10^{-7}\,T - 1.116 \times 10^{-5} \ (R^2 = 0.9951) \qquad \text{(A4)}$$

and for TP347H from reference 3 is:

$$\alpha_M = 1.694 \times 10^{-20}T^5 - 7.495 \times 10^{-17}T^4 + 1.222 \times 10^{-13}T^3 - 9.171 \times 10^{-11}T^2 + 3.572 \times 10^{-8}\,T - 1.115 \times 10^{-5} \ (R^2 = 0.9951) \qquad \text{(A5)}$$

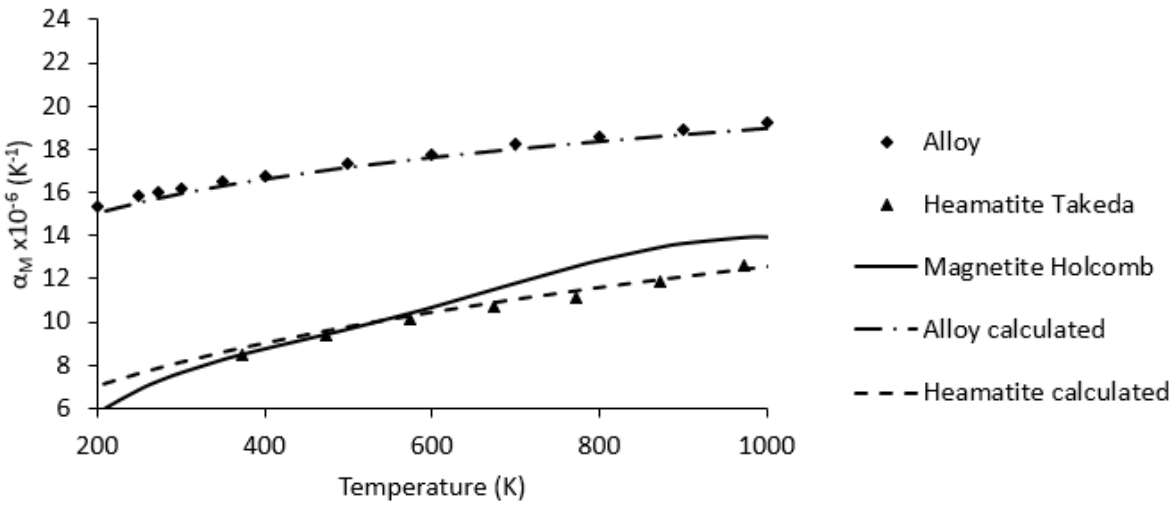

Figure A1. Plots of the thermal expansion coefficients, α_M, for the two iron-oxides formed in this study and the alloy TP347H [1-3].

The STORME technique has enabled the collection of the drop in temperature at which delamination resulted in the formation of a stable buckle, ΔT_{del}, as well as the temperature drop, ΔT_{prop}, at which the buckle becomes unstable and begins to grow. The ΔT_{spall}, the point at which spallation of an oxide fragment occurred, was also obtained. The thermal expansion coefficients for the alloy, magnetite and haematite were obtained for each sample and the difference between the values for the oxides, relative to the much thicker alloy, $\Delta\alpha$, calculated. These are presented for delamination, propagation and spallation in Tables A1, A2 and A3, respectively.

Table A1. Thermal expansion coefficients for TP347H, haematite and magnetite at the point of delaminationand buckle formation, α_{del}, with calculated $\Delta\alpha_{del}$ between alloy and each iron-oxide.

Time / hour	ΔT / K	α_{del} / x 10^{-6} K^{-1}			$\Delta\alpha_{del}$ / x 10^{-6} K^{-1}	
		Alloy	Fe_2O_3	Fe_3O_4	Alloy - Fe_2O_3	Alloy - Fe_3O_4
50	353	17.48	10.26	10.40	7.22	7.08
100	342	17.52	10.33	10.51	7.19	7.01
300	335	17.55	10.38	10.60	7.17	6.95
500	277	17.80	10.74	11.20	7.06	6.60
750	292	17.74	10.65	11.07	7.09	6.67
1000	406	17.23	9.91	9.87	7.32	7.36

Table A2. Thermal expansion coefficients, α_{prop}, for alloy, haematite and magnetite at point of propagation of the buckle with calculated $\Delta\alpha_{prop}$ between alloy and each iron-oxide.

Time / hour	ΔT / K	α_{prop} / x 10^{-6} K^{-1}			$\Delta\alpha_{prop}$ / x 10^{-6} K^{-1}	
		Alloy	Fe_2O_3	Fe_3O_4	Alloy - Fe_2O_3	Alloy - Fe_3O_4
50	371	17.40	10.14	10.22	7.26	7.18
100	370	17.40	10.15	10.23	7.25	7.17
300	335	17.55	10.38	10.60	7.17	6.95
500	330	17.58	10.41	10.65	7.17	6.93
750	328	17.58	10.42	10.67	7.16	6.91
1000	475	16.88	9.40	9.21	7.48	7.67

Table A3. Thermal expansion coefficients, α_{spall}, for alloy, haematite and magnetite at point of spallation of oxide fragments with calculated $\Delta\alpha_{spall}$ between alloy and each iron-oxide.

Time / hour	ΔT / K	α_{spall} / x 10^{-6} K^{-1}			$\Delta\alpha_{spall}$ / x 10^{-6} K^{-1}	
		Alloy	Fe_2O_3	Fe_3O_4	Alloy - Fe_2O_3	Alloy - Fe_3O_4
50	558	16.38	8.73	8.43	7.65	7.95
100	488	16.81	9.30	9.10	7.51	7.71
300	555	16.40	8.76	8.47	7.64	7.93
500	395	17.28	9.98	9.98	7.30	7.30
750	540	16.50	8.88	8.61	7.62	7.89
1000	519	16.63	9.06	8.81	7.57	7.82

References Appendix

[1] G. R. Holcomb, A review of the thermal expansion of magnetite, Materials at High Temperature, 36, (2019), 232-239.

[2] Takeda M, Onishi T, Nakakubo S, and Shinji Fujimoto. Physical properties of iron-oxide scales on Si-containing steels at high temperature. Mater Trans. 50 (2009) 2242–2246.

[3] P.D. Desai and C.Y. Ho, Thermal linear expansion of nine selected AISI stainless steels, American Iron and Steel Institute, CINDAS Report 51, April, 1978.

Figure 3

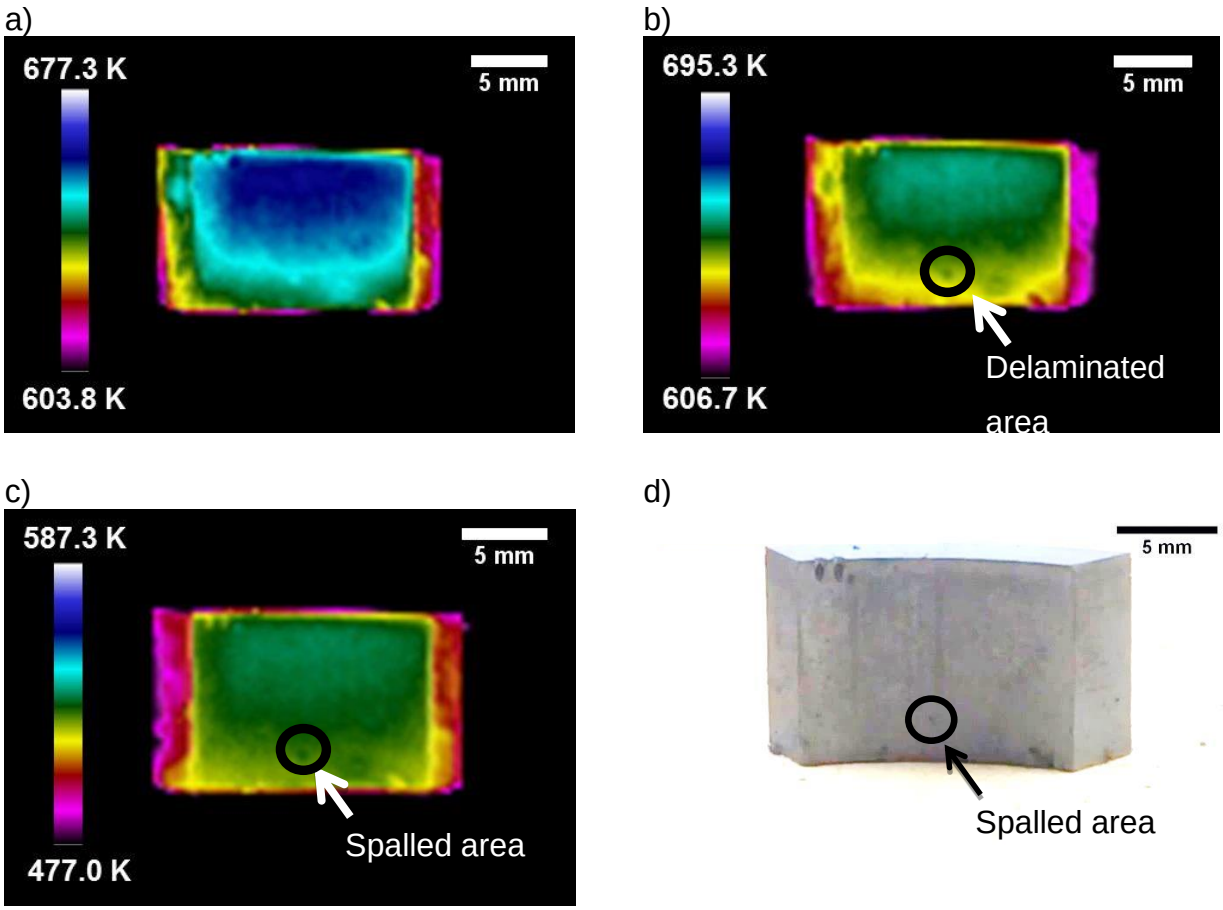

Figure 3. Thermographic images of the surface of TP347H FG during cooling after oxidation in air saturated steam at 923 K for 500 hours showing the initial site of spallation, circled, at (a) 1 second prior to the delamination event, (b) the time of delamination, (c) the time of spallation, (d) a snapshot taken from the video recording at the time of spallation.

Figure 4

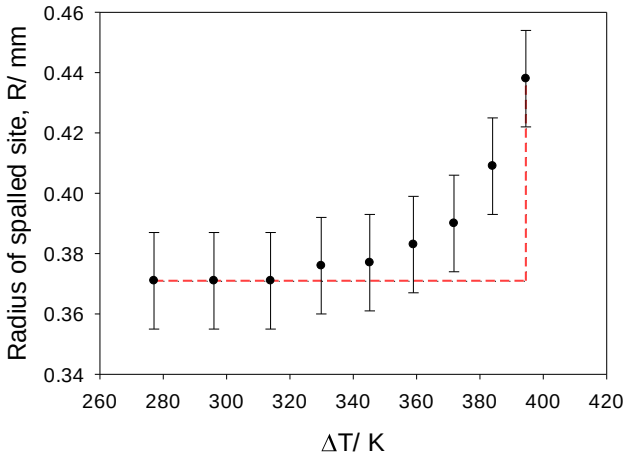

Figure 4. Plot of the radius of the buckled site shown in Figure 3 as a function of the temperature drop, ΔT, from the test temperature of 923 K following 500 hours of thermal exposure, showing that after formation there was a period of stability of the buckle followed by a gradual increase in area until spallation occurred. The level of accuracy of these measurements is indicated by the error bars. The horizontal dashed line emphasises the point at which propagation begins and the vertical line represents the spallation event.

Figure 5

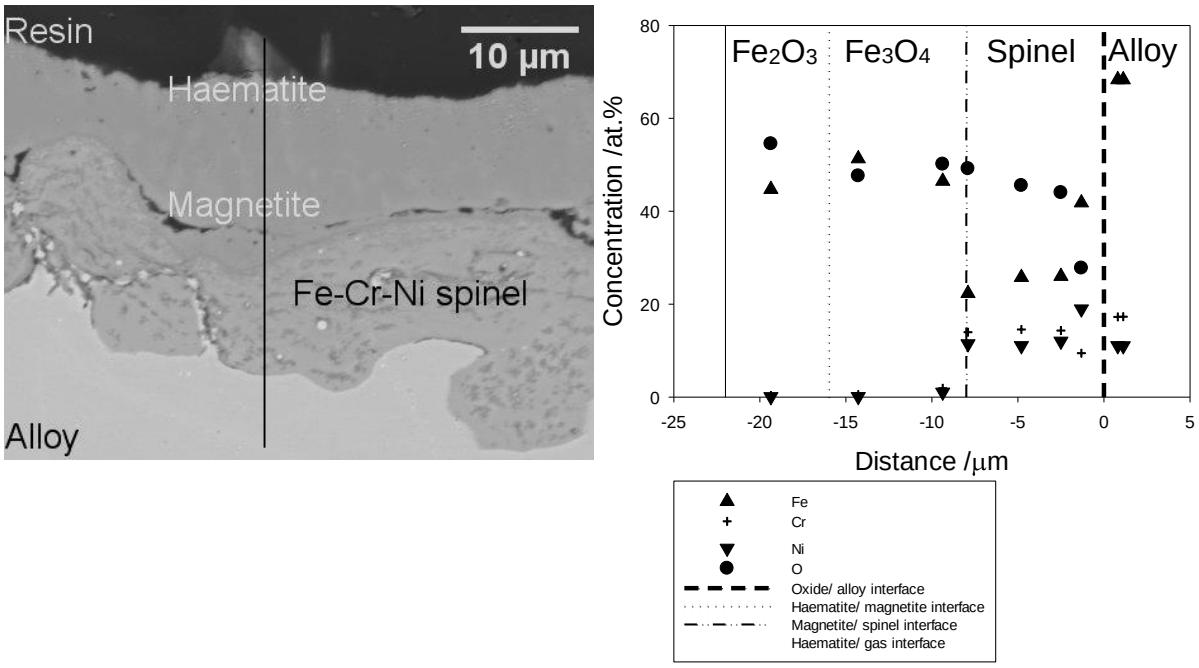

Figure 5. Back scattered electron (BSE) micrograph of TP347H FG exposed to air saturated steam for 100 hours at 923 K and the corresponding concentration profile where Cr and O are measured using WDS analysis showing the formation of a layered oxide structure at the site indicated by the solid line on the micrograph.

Figure 6

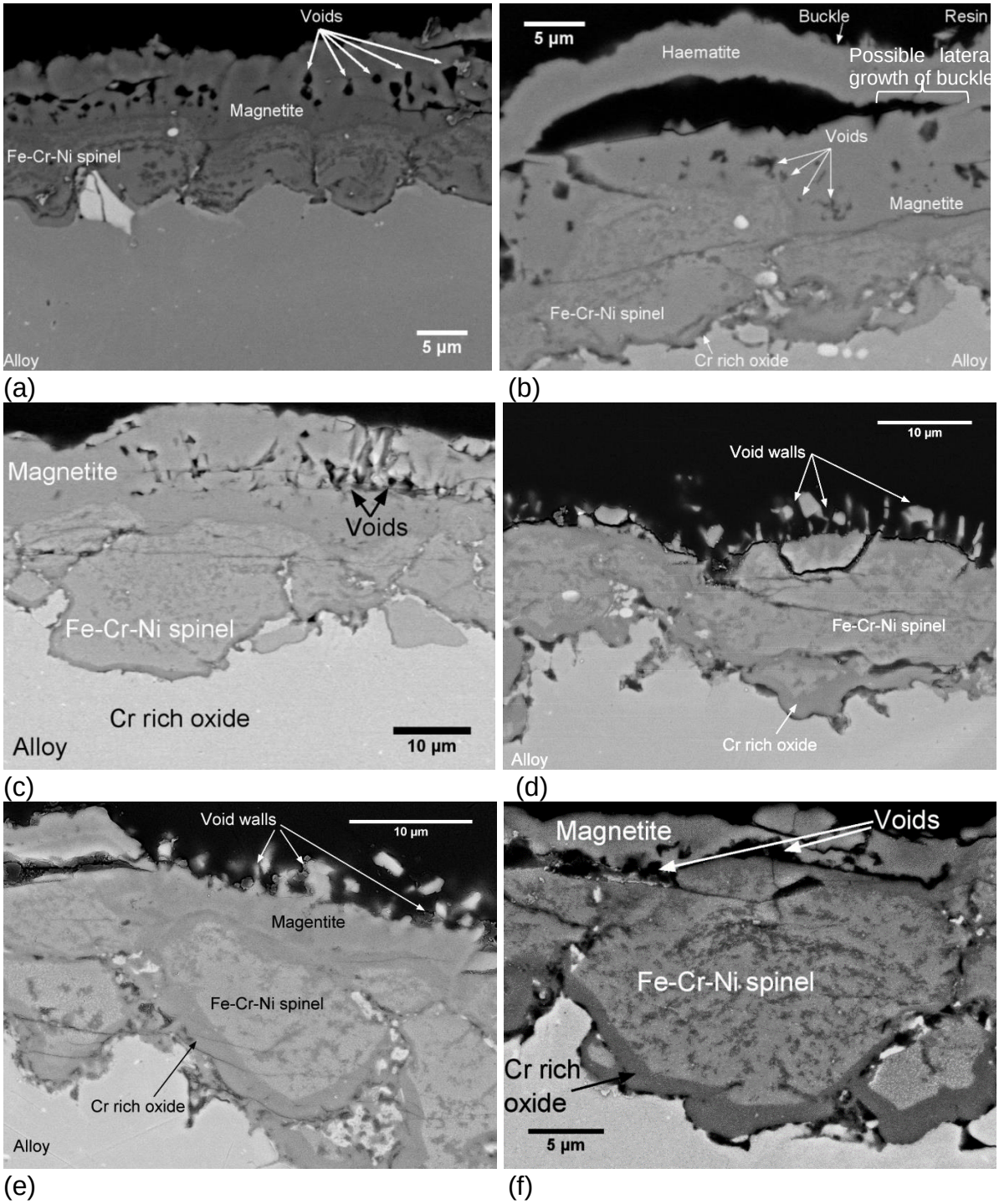

Figure 6. Cross-sectional BSE micrographs of TP347H FG post oxidation in air saturated steam at 923 K for (a) 50 hours, (b) 100 hours, (c) 300 hours, (d) 500 hours, (e) 750 hours and (f) 1000 hours.

Figure 7

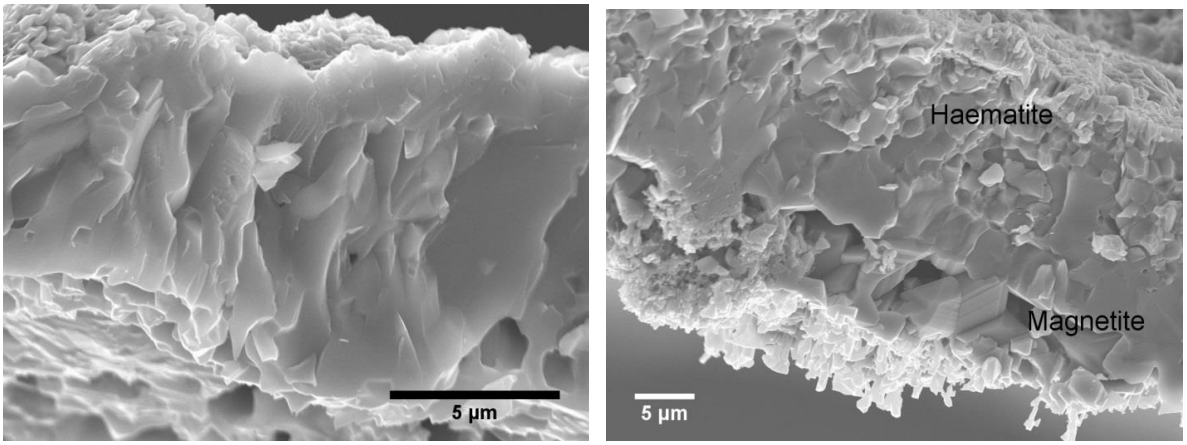

(a) (b)

Figure 7. Secondary electron (SE) images of spalled particles from TP347H FG oxidised in air saturated steam at 923 K for (a) 50 hours and (b) 500 hours.

Figure 8

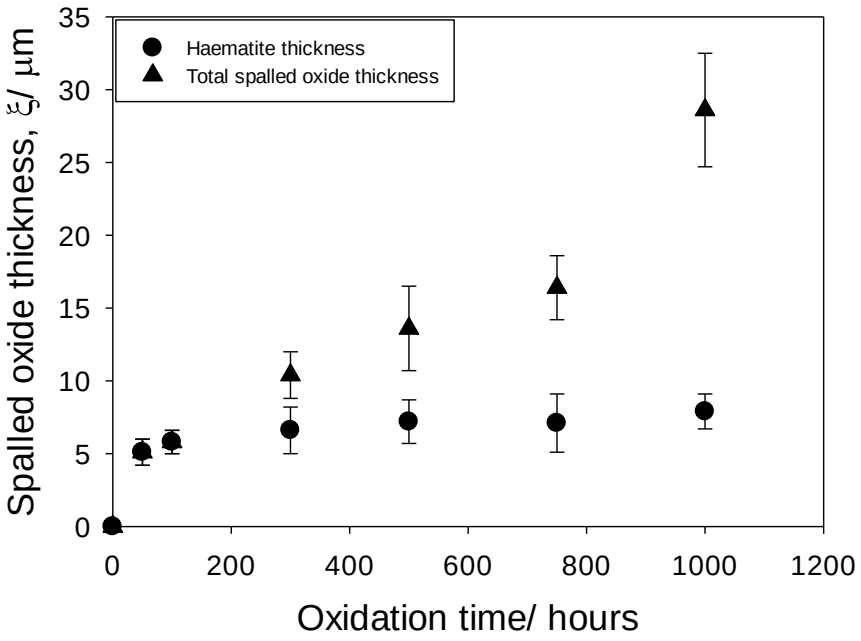

Figure 8. A plot of average spalled oxide thickness as a function of oxidation time including error bars which correspond to ± one standard deviation, based on 20 measurements along the spalled particle.

Figure 9

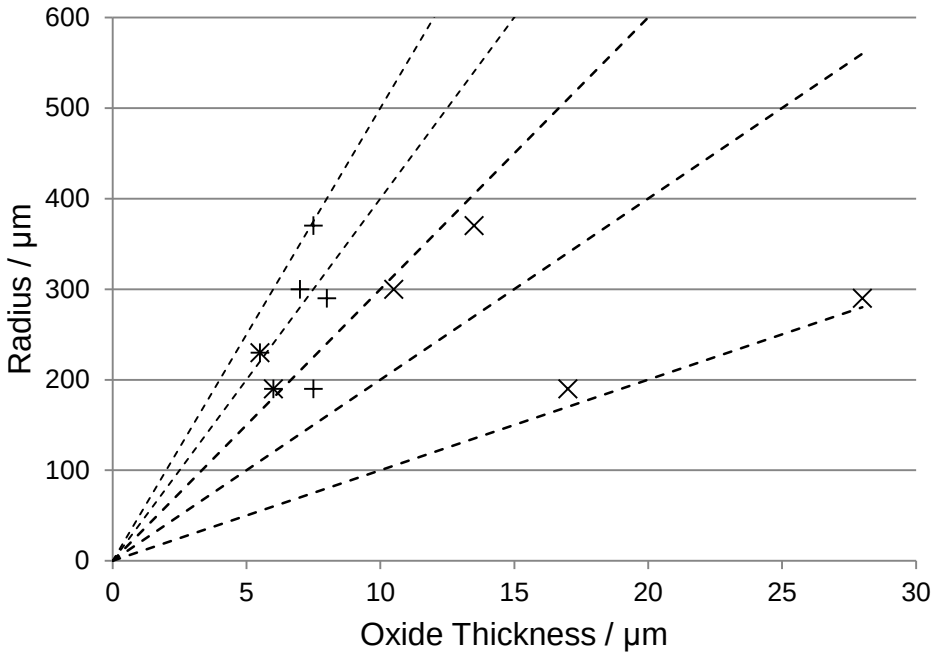

Figure 9. Plot of radius of delamination against oxide thickness, with values assuming the theoretical ratios of 1:50 to 1:10 marked by dashed lines.

Figure 10

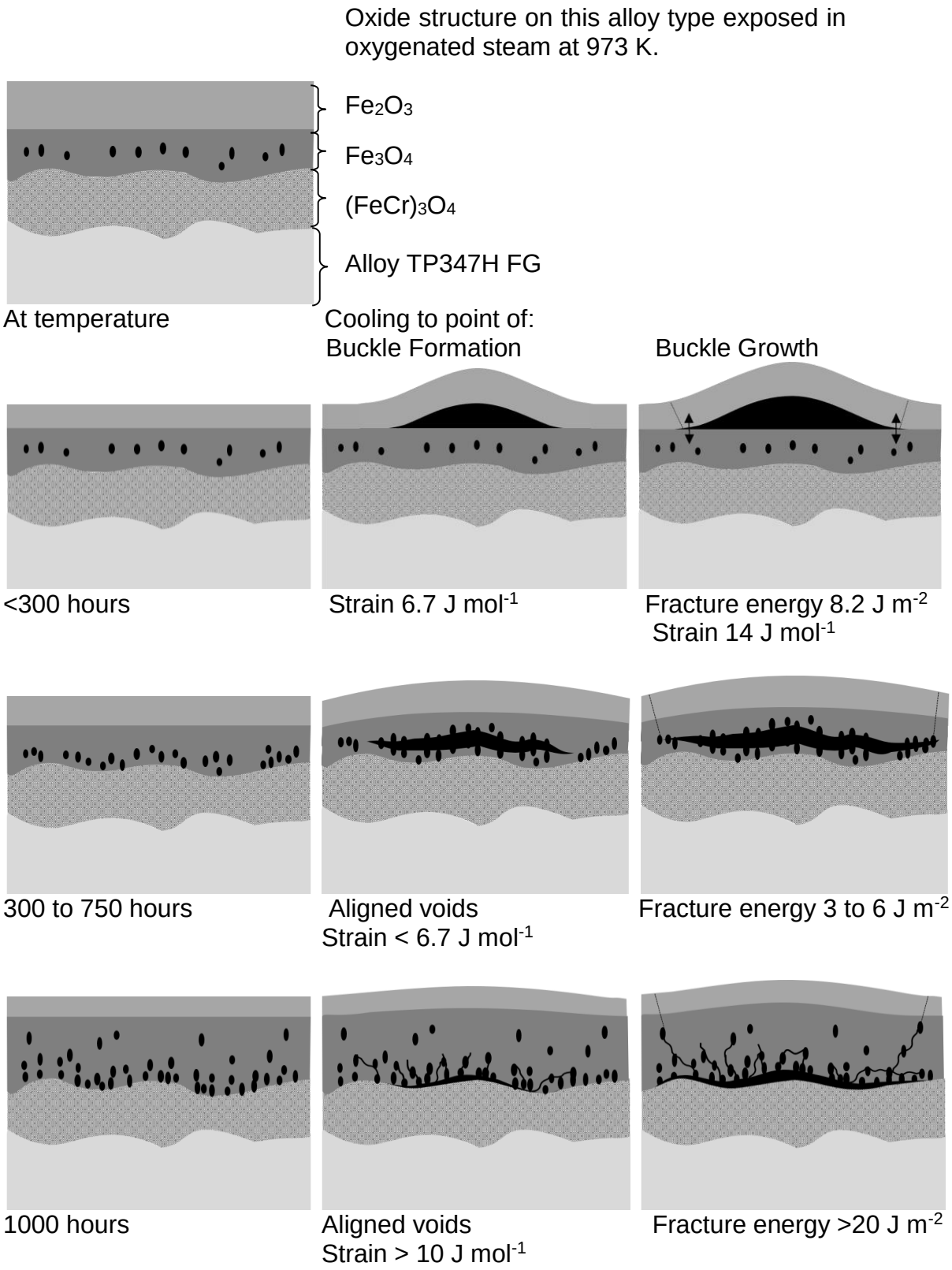

Figure 10. Schematic diagrams showing the sequence of events leading to spallation of the initial oxide fragment following increasing exposure to steam conditions at 973 K, showing pore development and delamination leading to the formation of a buckle.

Figure 11

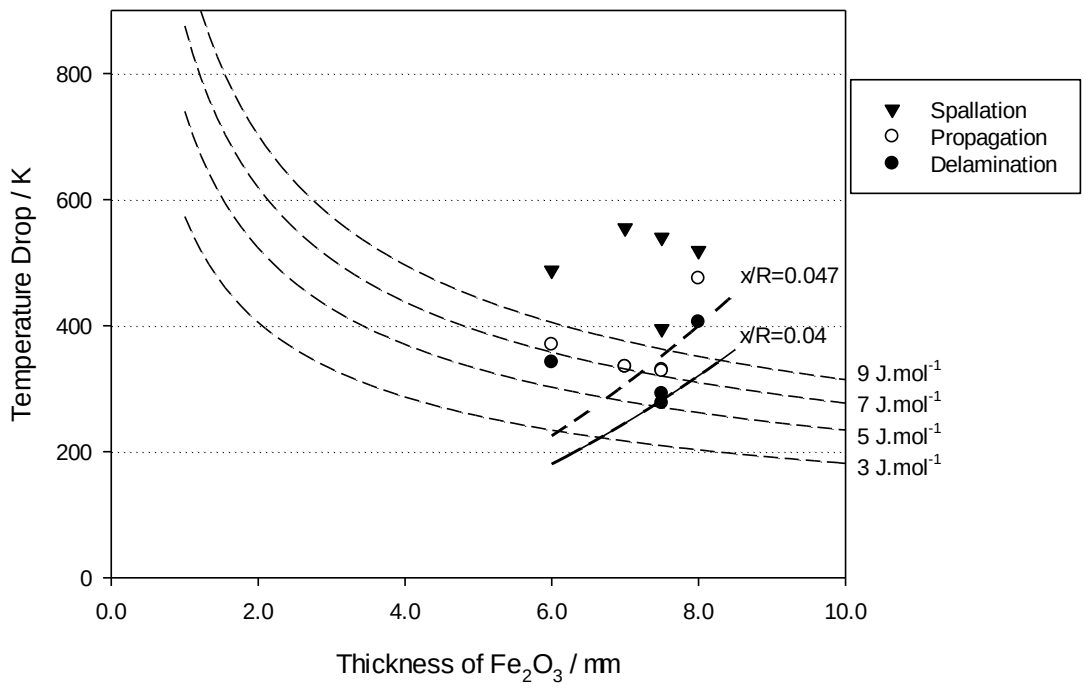

Figure 11. Spallation map for TP347H showing the ΔT for delamination, propagation and spallation events against Fe_2O_3 for the first spallation event, also plotted are Equation 3 using fracture energies of 3, 5, 7 or 9 $Jmol^{-1}$, decreasing dashed lines, and Equation 4 indicating a change in spallation mechanism at a ξ/R of 0.04, details of the values used for each equation are given in the text.

Figure 1

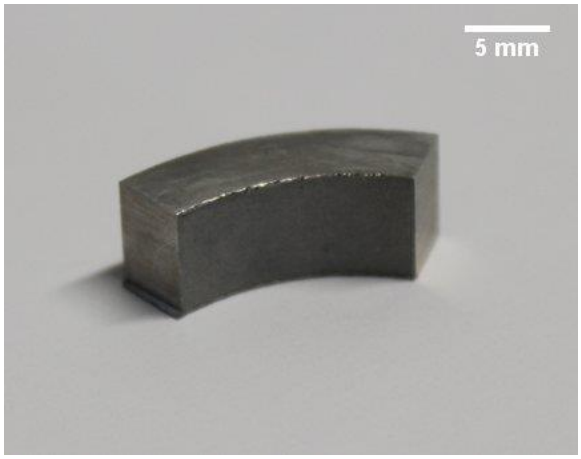

Figure 1. Photograph of a sample of TP347H FG boiler tubing used for steam oxidation experiments positioned for examination of the concave surface during the cooling stage.

Figure 2

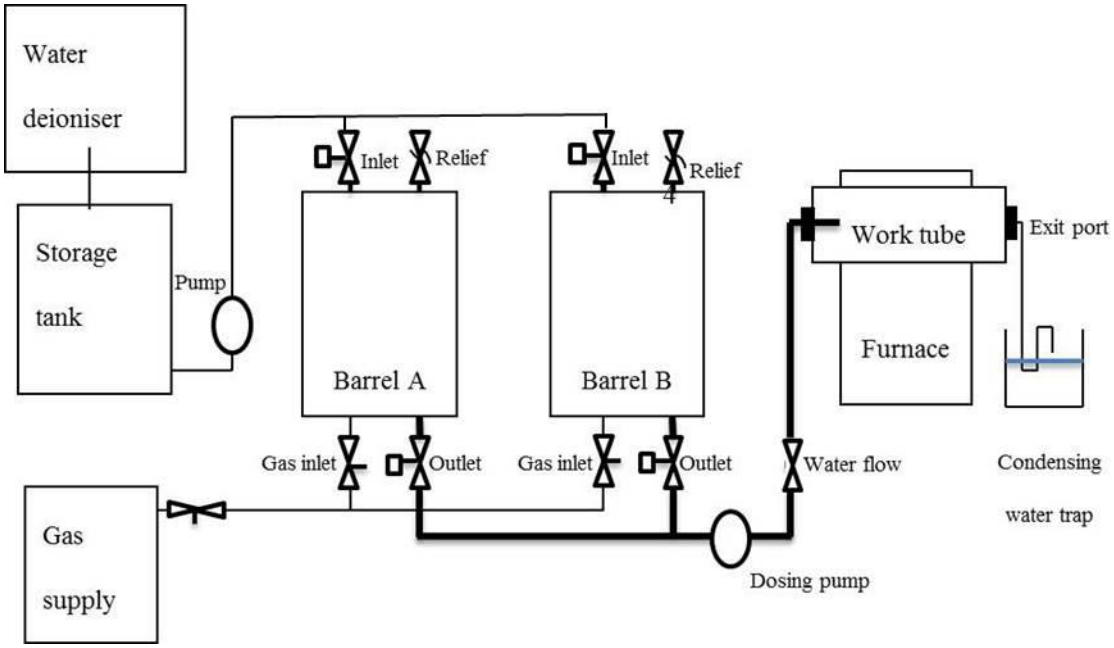

Figure 2. Schematic diagram of the steam oxidation rig.

Table

Metallurgy and Materials
The University of Birmingham
Birmingham B15 2TT

Dear Editor,

There is no conflict on interest.

Yours faithfully

Dr Mary Taylor

Authors' statement

Dear Sir or Madam

This is to certify that all the **authors** have seen and approved the final version of the manuscript being submitted. The article presents the **authors**' original work and it has not been published before and is not under consideration for publication elsewhere.

Yours faithfully

Dr. Mary Taylor

School of Metallurgy and Materials,

University of Birmingham,

B15 9HB

UK.